



Long-Term Time Series Analysis of Land Cover Changes in an Arid Environment Using Landsat Data: A Case Study Of Hamoun Biosphere Reserve, Iran

Rasoul Kharazmi¹ , Mohammad Reza Rahdari^{2*}  ,
Andrés Rodríguez-Seijo^{3, 4, 5} , Mohamed Elhag^{6,7,8,9} 

¹ Soil and Water Research Institute, Agricultural Research, Education and Extension Organization (AREEO), Karaj, Iran.

² Faculty of Agriculture, University of Torbat Heydarieh, Torbat Heydarieh, Iran. Email: rahdarimr@torbath.ac.ir.

³ Area de Edafología, Departamento de Biología Vegetal e Ciencia do Solo, Faculdade de Ciencias, Universidade de Vigo, As Lagoas s/n, 32004, Ourense, Spain.

⁴ Interdisciplinary Centre of Marine and Environmental Research (CIIMAR), University of Porto, Terminal de Cruzeiro do Porto de Leixões, Av. General Norton de Matos s/n, 4450-208, Matosinhos, Portugal.

⁵ Department of Biology, Faculty of Sciences, University of Porto, Rua do Campo Alegre, 4169-007, Porto, Portugal

⁶ Department of Hydrology and Water Resources Management, Faculty of Meteorology, Environment & Arid Land Agriculture, King Abdulaziz University Jeddah, 21589, Saudi Arabia.

⁷ The State Key Laboratory of Remote Sensing, Aerospace Information Research Institute Chinese Academy of Science (CAS), Beijing 100101, China.

⁸ Department of Geoinformation in Environmental Management, CI-HEAM/Mediterranean Agronomic Institute of Chania, Chania 73100, Greece.

⁹ Department of Applied Geosciences, Faculty of Science, the German University of Technology in Oman, Muscat 1816, Oman.

Article Info.

Article type:
Research Article

Article history:
Received: 17 Feb. 2023
Received in revised from: 09 Mar. 2023
Accepted: 06 May 2023
Published online: 27 June 2023

Keywords:
Environment monitoring,
Vegetation Indices,
Image Classification,
Landsat,
Multispectral Images.

ABSTRACT

Change detection of lakes is important to monitor ecosystem health and wind erosion process in arid environments. The main purpose of this research is to evaluate unsupervised classification based on vegetation indices to monitor Land cover changes (LCCs). The Hamoun Biosphere Reserve is located in the east of Iran and is considered one of the most important wetlands in the center of the Iran Plateau. To detect land cover changes, using Landsat images from the 1990s, 2000s, 2010s and 2020s ground control points (GCP) and spectral profiles, four major land cover classes were obtained (sparse vegetation, dense vegetation, bare land, and water bodies). To create AOIs, the pure pixels were selected using obtained spectral profiles of the main land types by GCPs in 2020. The separability of representative AOIs by classes was examined by Jeffries–Matsushita distances and scattering ellipse parameters. A maximum likelihood classifier (MLC) was applied to Landsat images in 2020 with an overall accuracy of 93% and a Kappa statistic of 0.90. Subsequently, based on Soil Adjusted Vegetation Index (SAVI) maps, as additional input data, unsupervised classification was used to classify the same images in 2020. The observed accuracy and kappa statistic of the used classification technique was up to 0.91 and 0.89 respectively. The finding indicated that in 2000, the area of arid land increased (90% of all areas) and became a major land use type, whereas water bodies (74% of all areas in the 1990s) reached zero in this year. Yearly water body changes revealed a severe dryness condition in this wetland. After 2000, in most cases in subsequent years, the water body completely dried up and in the seasonally flooded years, it did not exceed 10% of the total wetland's area. On the other hand, before 2000, on average, 60% of the wetland's area was dominated by the water class. Our study showed that in the time series without GCP for monitoring past changes, an unsupervised SAVI-based technique could provide acceptable accuracy in this region.

Cite this article: Kharazmi, R., Rahdari, M.R., Rodríguez-Seijo, A., Elhag, M. (2023). Long-Term Time Series Analysis of Land Cover Changes in an Arid Environment Using Landsat Data: A Case Study Of Hamoun Biosphere Reserve, Iran. *DESERT*, 28 (1), DOI: 10.22059/jdesert.2023.93547



1. Introduction

Environmental problems due to climatic factors and anthropogenic activities have long only been considered for dry land ecosystems (Karmaoui, *et al.*, 2014; Li, *et al.*, 2016; Groisman, *et al.*, 2018; Jiang, *et al.*, 2018; Xu, *et al.*, 2019; Chen, *et al.*, 2020; Sahabi and Moallem Banhangi, 2022). Lake area fluctuations are an important proxy of climate and environmental changes on a regional scale in dryland ecosystems (Mason, *et al.*, 1994; Kang, *et al.*, 2015; Yang, *et al.*, 2020; Rahimi, *et al.*, 2021; Sahabi, *et al.*, 2022). Dryland lakes, as a major water reserve in arid regions, play a key role in local socio-economic activity (Bai, *et al.*, 2011; Wang, *et al.*, 2021; Lu, *et al.*, 2022).

Land cover, together with land use type, forms a pattern of view in environmental studies (Bashiri, *et al.*, 2017; Rousta *et al.*, 2018). Determination of specific land cover and land use spatial patterns is essential to assess the landscape as well as develop better facilities for land management and conservation goals (Serban, *et al.*, 2020; Pandey, *et al.*, 2021; Mansourmoghaddam *et al.*, 2021). The acquisition of data that describe ecosystem health plays an important role in land management. However, obtaining field data is often difficult and limited when assessing and monitoring the land cover on a global and regional scale (Gong, *et al.*, 2013; Gao, *et al.*, 2020; Liu, *et al.*, 2020).

Remote sensing is a useful technology that facilitates data acquisition for environmental observation (Alavi Zadeh, *et al.*, 2013; Yuan, *et al.*, 2020; Li, *et al.*, 2020). It plays a significant role in environmental monitoring and the management of extensive areas by creating a broad as well as integrated vision of the region and providing facilities for recognizing land cover and land use spatial patterns (Nagendra, *et al.*, 2013; Kennedy, *et al.*, 2015; Tmusic, *et al.*, 2020). Such features as wide viewing, using different parts of the electromagnetic spectrum to record data about phenomena; above all, they are relatively low-cost and rapid, which contributes to the widespread use of this method (Alavipanah, *et al.*, 2007; Chen, *et al.*, 2019). The main characteristic of remote data sensing is its digitization, which provides the feasibility of object, the analyses and reflects the state as well as changes in land cover/land use mosaic (Liu, 2015; Tahsin, *et al.*, 2021).

Satellite images should be processed and classified to create thematic maps of land cover plus land use for specific environmental studies. The successful classification depends on the accurate digital distinction of spectral reflections of categorical events (Yang, *et al.*, 2002; Dhingra, *et al.*, 2019; Kaselimi, *et al.*, 2022).

Various classification methods for LCC analysis, based on remote sensing data, have been implemented and deployed (Zhao, *et al.*, 2017; Abdollahi, *et al.*, 2022; Yousefi, *et al.*, 2022). Typically, classification is performed on a pixel basis in two different ways: supervised and unsupervised (Long, *et al.*, 2002; Mohammady, *et al.*, 2015; Kalidhas, *et al.*, 2022). In supervised classification, pixels in the image are segregated into known classes based on their spectral values, while in unsupervised cases, pixels are segregated as groups or clusters based on the pixel values themselves (Jensen, 2018; Berry, *et al.*, 2020). The basic principle is that similar pixel values should be grouped into a separate class. This method is used when little or no information is available on the land cover classes (Alloghani, *et al.*, 2020).

Some studies have recently applied various methods for classifying wetland land cover changes (LCCs). For example, Soliman and Soussa (Soliman, *et al.*, 2011) performed a supervised maximum likelihood classification and the post-classification comparison change detection to monitor wetland cover changes in the Nile swamps. The authors processed three Landsat multispectral satellite imageries and classified land covers into five main land cover classes. They concluded that the use of remote sensing algorithms and post-classification methods can detect the area of changes in classes and reveal ecosystem dynamics. Mousazadeh

et al. (2015) performed a supervised maximum likelihood classification for the LCC of the Anzali International coastal wetland; they stated that supervised classification methods can be useful for monitoring and behavior analyses of other Iranian wetlands. Chouari *et al.* (2021) applied a maximum likelihood classification algorithm for identifying different land cover classes of the Al-Asfar wetland. Additionally, the author proposed the normalized difference vegetation index (NDVI) and the normalized difference water index (NDWI) for separating green crop cover areas and water features from other land covers. They also proposed an unsupervised ISO-cluster classification method to reveal changes in the different resulting classes in the study area. Talukdar *et al.* (2021) employed supervised and machine learning classifiers for the mapping of the wetland inundation area using Artificial Neural Network (ANN), Random Forest (RF), Support Vector Machine (SVM), Maximum Likelihood Classifier (MLC), Parallelepiped (PP), and Spectral Information Divergence (SID). Their study showed that SVM has better accuracy than the other methods. Ahmed *et al.* (2021) presented a wetland classification by applying unsupervised K-means cluster classification and supervised SVM algorithms, using Landsat data to model NDVI and NDWI as auxiliary data. Their results indicated that the employed methodology was a simple and robust classification based on advanced unsupervised and supervised algorithms. The literature reviews suggested that -based remote sensing methods have resulted in several wetlands LCC monitoring studies. These methods can well represent the wetland dynamics for sustainable wetland management.

One of the main problems in LCC monitoring in regions such as the Hamoun Biosphere Reserve is the lack of accurate georeferencing information from the past. Although it is time-consuming and difficult to access the study region, satellite imagery and remote sensing technology make it possible to analyze the situation and visualize past LCCs in areas where field data are not available. Additionally, using auxiliary data such as vegetation indices can detect LCCs in high accuracy (Almalki, *et al.*, 2022). The obtained information can be used for developing better LCC management strategies (Lv, *et al.*, 2022; Opedes *et al.* 2022). The number of studies on LCCs using Landsat images has been increasing substantially since 2008 (Zhu, *et al.*, 2020; Kumar, *et al.*, 2021), and many studies have been conducted to evaluate LCCs with the support of Landsat images (Muttitanon, *et al.*, 2005; Sonnenschein, *et al.*, 2011; Hansen, *et al.*, 2012; Nutini, *et al.*, 2013; Venter, *et al.*, 2020; Wulder, *et al.*, 2022).

Different image classification techniques are used in almost all thematic studies that implement the use of remote sensing data. Currently, we have a considerable amount of satellite imagery available in near real-time mode for monitoring purposes and massive data available as an archive for retrospective analysis as well as the study of environmental interdependencies.

This situation has led to the implementation of highly automated machine learning techniques, which could be applicable for operations with big data (or at least big-size datasets) and could generate valuable, comparable, and representative results (Li, *et al.*, 2020; Alshahrani, *et al.*, 2021). Unfortunately, it is unfeasible to build fully automated and autonomous analysis techniques, mainly because of the high dynamics and high complexity of the environment as well as the understudied details of numerous environmental processes.

In recent years, the Google Earth Engine platform (GEE) has been able to facilitate many satellite image processing analyses (Pande, 2022). One of the advantages of this platform is its extensive library of spatial data which allows users to perform complex analyses on satellite images (Yang, *et al.*, 2022). The free-to-use GEE is a cloud computing platform that provides the possibility of extracting water resource information such as water surface area, runoff, revealing flooded areas, etc. (Wang, *et al.*, 2020; Jiang, *et al.*, 2021).

The arid Iranian plateau is a vulnerable ecosystem (Rastegar-Pouyani, *et al.*, 2015), and the Hamoun Biosphere Reserve, located in the dry part of the central Iranian plateau, is a terrestrial

and wetland ecosystem. Under the harsh environmental conditions of a hot and dry climate, this lake plays an important role in the environment and human living conditions in eastern Iran and western Afghanistan (Dahmardeh, et al., 2019; Sanadgol, et al., 2022). Over the last two decades, the Hamoun Biosphere Reserve has experienced severe drought due to anthropogenic activities (Kharazmi, et al., 2018; Ehsani, et al., 2021). Thus, it is vital to study this lake's dynamics to understand the patterns of changes and the impacts on regional socio-economic activities.

Our study investigated the spatial and quantitative dynamics of LCC in the Hamoun Biosphere Reserve using Landsat data by developing an algorithm for selecting AOIs and evaluating the results of supervised plus unsupervised classification based on vegetation indices, providing information about the recent and historical LCC conditions of the wetland. Additionally, we searched for ways to use unsupervised classification as a reliable automated method for monitoring LCCs in dry-land lakes.

2. Material and Methods

2.1. Study area

Hamoun Biosphere Reserve is a segment of the Hamoun wetlands located in the East of Iran at the end of Hirmand Basin, one of the driest regions in the world (Fig. 1), between $30^{\circ} 10'$ and $31^{\circ} 14'$ of North latitude and $60^{\circ} 58'$ and $61^{\circ} 20'$ East longitude. The study area covers $1,930 \text{ km}^2$. Low precipitation and high evaporation are the main climatic character of this region. The annual rainfall in the Sistan Basin is about 50 mm. One of the main factors affecting weather conditions in the region are strong 120-day winds, which make Sistan one of the windiest arid regions in the world (Rashki et al., 2013; Rezaei and Ghofranfarid, 2018). Due to strong winds and temperature, the average annual evaporation in this area is up to 4000 mm (Vekerdy *et al.*, 2006).

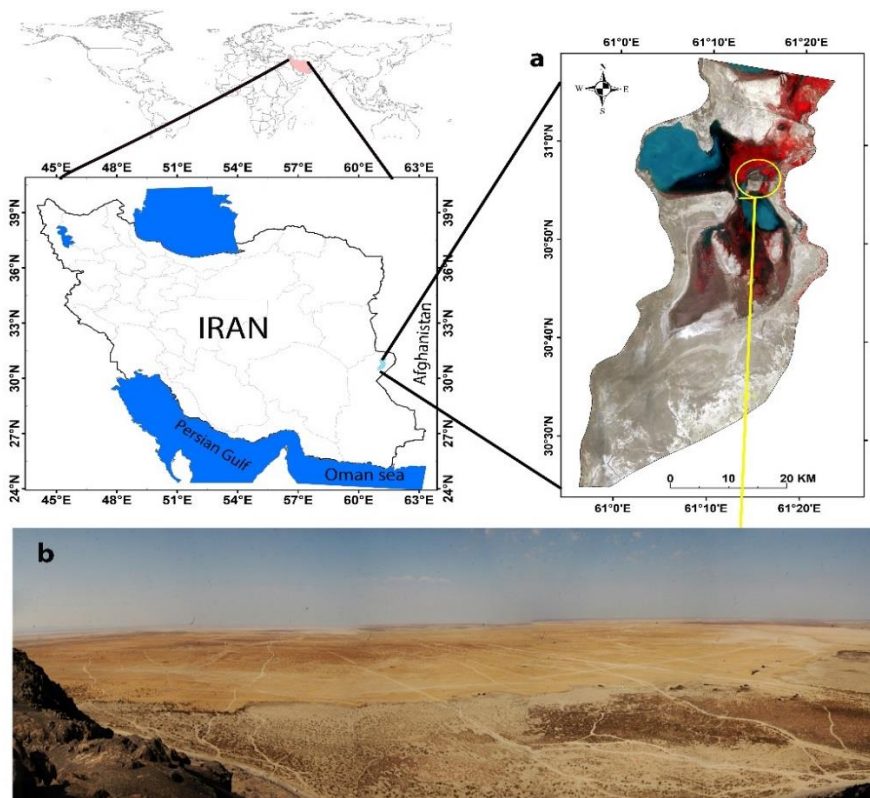


Fig. 1. Location of the study area with false color of Landsat OLI in 2020 (a) and a view of the dried bed of wetland(b) (photo by Mehdi Kavei)

Consequently, full-fledged life and economic activities are possible only if external sources of water are available. The main water source of Hamoun Biosphere Reserve is the Hirmand River, which brings fresh snow and meltwater from the Hindu -Kush Mountains making this wetland the only source of viable habitats in the region. This wetland provides water for agricultural activities, livestock grazing, and fishing.

2.2. Data sources

Since 1972, the Landsat satellite has continuously been collecting land surface data and providing valuable data for LCC monitoring. Annual visual interpretation of the Landsat series in this region indicated that, in the 2000s, this lake had become bare land, and three periods could be defined (Vekerday *et al.*, 2006; Kharazmi *et al.*, 2018):

1-The period in which the Hamoun Biosphere Reserve was a permanent lake and water was the main land cover (1990–2000),

2-Dry period, in which the lake totally changed to bare land and became a seasonal lake (2000–2010),

3- The period in which the balance of inflow and outflow-maintained vegetation cover (2010–2020).

According to these periods, Landsat data were collected in 1990, 2000, 2010, and 2020 to monitor decadal LCC (Table 1). Based on Landsat data for the relevant years, land type trends were analyzed throughout the territory. Previous studies have demonstrated that due to climatic factors, the dynamic changes of wetlands in May and June are more significant than those in other seasons (Wang, *et al.*, 2019; Jiang, *et al.*, 2021). Thus, to detect decadal LCCs, all analyzed time series images were selected in June.

Table 1. Data used in this study.

Satellite Data	Path/Row	Resolution	Date	Cloud cover
Landsat-5 (TM)	157/039	30 m	12 JUN 1990	<10%
Landsat-5 (TM)	157/039	30 m	7-JUN 2000	<10%
Landsat-5 (TM)	157/039	30 m	19-JUN 2010	<10%
Landsat-8 (OLI)	157/039	30m	24-JUN 2020	<10%
Other data				
Google Earth		Varying resolution	2020	
Field observation			JUN 2020	

2.3. Image pre-processing

The software ERDAS Imagine 2014 and ENVI 5.3 were used for image processing. The Landsat collection pre-processing involves geometric and radiometric calibration, top of the atmosphere reflectance (TOA), and surface reflectance (Ali, *et al.*, 2018). Geometric correction of images was done by the image-to-image model (Vekerdy, *et al.*, 2006; Maleki, *et al.*, 2019), using 21 control points with an accuracy of 0.3 to 0.5 pixels. Additionally, radiometric and atmospheric correction of all images was applied using the module FLAASH ENVI 5.3 and pixel values were converted to reflectance values, which range from 0 to 1 (Maas, *et al.*, 2010; Zhai, *et al.*, 2022).

2.4. Field data

To determine the characteristics of land cover classes, all major land covers were acquired by conducting field sampling in June 2020, analyzing topographic maps, and examining the

spectral characteristics of land cover, followed by visual interpretation in Google Earth Pro (Gill, *et al.*, 2010). The land cover classes were aggregated into four general groups (Table 2).

Table 2. The land covers types at the study area

No	Land Cover Type	Short Description
1	Water	Territories covered with deep water
2	Bare land	Territories covered with vegetation less than 10 %.
3	Dense Vegetation	Rangelands and territories are covered with canopy vegetation of more than 20 %.
4	Sparse vegetation	Rangelands and territories are covered with canopy vegetation between 10- 20 %.

2.5. Classification

The reliability of change estimates, in this case, depends on the image classification accuracy (Zhai, *et al.*, 2019).

In a supervised classification, the quality and quantity of the training samples are important issues. Thus, their appropriate preparation is a crucial step in the workflow (Malinowski, *et al.*, 2020).

The main requirement for the areas of interest (AOI) polygons is their representativeness. Sample pixels must correspond to the same class on the ground. In this study, to create AOIs, the pure pixels were selected using obtained spectral profiles of the main land types in 2020. Next, the pixels with similar spectral characteristics around these control points were selected using the "Region Grow" properties tool in ERDAS Imagine; wherein, depending on the size of similar areas, 100 to 400 pixels were grouped in a single AOI. For each class, 10 AOIs were selected in different parts of the image, after which these AOIs were combined into one class.

One of the main characteristics of the vegetation cover in arid regions is its sparseness (Zhu, *et al.*, 2022). When selecting samples, it is necessary to validate the spectral separability between vegetation and non-vegetation classes. Signature separability is calculated as the statistical difference between two spectral signatures. The estimation of the separability between classes is examined by Jeffries–Matsushita (JM) distance, which also considers the values of dispersion (covariance) within the samples.

$$JM_{ij} = \sqrt{2(1 - e^{-\alpha})} \quad (1)$$

$$\alpha = \frac{1}{8} (\mu_i - \mu_j)^T \times \left(\frac{C_i - C_j}{2} \right)^{-1} \times (\mu_i - \mu_j) + \frac{1}{2} \ln \left(\frac{|C_i - C_j|}{\sqrt{|C_i| \times |C_j|}} \right) \quad (2)$$

Where, μ_i and μ_j represent the mean values, and C_i and C_j denote the covariance matrices of the classes i and j respectively (Swain and Davis 1978; Dabboor, *et al.*, 2014).

The JM distance has an upper and lower bound between 0 and 1414. If the calculated divergence is equal to the corresponding upper bound, then the signatures will be considered completely separable in the studied bands (Viennois, *et al.*, 2016; Jensen, 2018).

Additionally, to assess the quality of created AOIs, scattering ellipses parameters were calculated from the brightness values of sample pixels, along with the average values and standard deviations of the pixels stored in the files of training samples. This parameter is used to represent ellipses of different classes in a two-dimensional feature space (Xu, *et al.*, 2019). In this method, if the ellipses in the scatterplot have significant overlap, then the pixels

representing these samples cannot be separated by spectral characteristics in these zones.

The test areas (AOIs) belonging to each class were selected, and the land cover was determined further based on the results of the field observations in 2020. For each land use class, the test areas were divided into two groups: training and control. Image classification was performed using the ERDAS Imagine MLC algorithm with training samples.

To ensure a unified approach to assessing classification accuracy, the Maximum Likelihood Classifier (MLC) was applied to the 2020 time-series image. MLC was recommended to analyzing satellite images in some studies in dry land ecosystems and compared to other classification algorithm, this algorithm has most accurate results in dry lands (Ajaj *et al.*, 2017; Kharazmi *et al.*, 2018; Chughtai *et al.*, 2021; Stavi *et al.*, 2023). MLC is a supervised classification technique that works based on multivariate probability density function of classes. The MLC method is based on the concept of the likelihood function of a reference sample in class C (Ahmad and Quegan, 2012; Gaikwad, *et al.*, 2019). Based on the training sample data, the mean measurement vector (M_C) and the covariance matrix (V_C) are calculated for each class (C) plus spectral range (K). According to the obtained results, pixel X belongs to class C if: $P_C > P_i$, where $i=1, 2, 3 \dots m$; m is the number of classes; P_i denotes the probability that the given class exists. In this case, the probability of P_C is determined by the following formula:

$$P_C = \left(-0.5 \times \log_e(\det(V_C)) \right) - \left[0.5 \times \frac{(X-M_C)^T \times (X-M_C)}{V_C} \right] \quad (3)$$

In this algorithm, each selecting training class should follow a Gaussian distribution (Mishra, *et al.*, 2017).

Due to lack of ground information in all-time series, we used unsupervised method to classify the images without GCPs. Since in this study, we focused on comparing and estimating the accuracies of supervised as well as unsupervised classification techniques in detecting LCC's, we decided to use vegetation indices as auxiliary data for validation purposes. For this purpose, the SAVI (Othman, *et al.*, 2018) was calculated for the 2020 satellite imagery scenes, and subsequently unsupervised classification was performed based on the results of this index.

In our case, the SAVI was used for detecting LCC's and assessing the land cover classification quality. This vegetation index gives the most accurate correlations with the total biomass of vegetation in dry region (Huete, 1988; Bezerra, *et al.*, 2022).

$$SAVI = \frac{(NIR-RED)}{(NIR+RED+L)} \times (1 + L) \quad (4)$$

Where,

NIR = reflectance value in the near-infrared band of the multispectral imagery;

RED = reflectance in the red band;

L = soil brightness correction factor, which varies depending on the amount of green vegetation between 0 in highly vegetated regions and 1 in regions without green vegetation, with a default value of 0.5.

The efficiency of the SAVI application for the selected study region is explained by the fact that the SAVI minimizes the variations of spectral vegetation properties, which are influenced by different types of soil (Kharazmi, *et al.*, 2016; Karkon Varnosfaderani, *et al.*, 2017). To determine and estimate the accuracy of the SAVI-based classification technique used for unsupervised classification, supervised classification of the same satellite imagery scenes was performed. For this purpose, we used the field observation and sampling data collected at the previous stages of our research (Yuan, *et al.*, 2005; Sharifikia, *et al.*, 2017) as well as from the Google Earth Pro archive.

2.6. Water body extraction

Annual water body area of wetland was extracted using modified normalized difference water Index (mNDWI) in GEE platform in June of each year using Landsat images (Khalid et al., 2021; Condeça et al., 2022). This index was developed to highlight the water features in the images from the green and Shortwave-Infrared (SWIR) bands, which can separate water areas from the other classes with acceptable accuracy (XU, 2006; Rad, et al., 2021).

$$\text{mNDWI} = \frac{(\text{GREEN} - \text{SWIR}) - 1}{(\text{GREEN} + \text{SWIR}) - 1} \quad (5)$$

GREEN = reflectance value in the green band of the multispectral imagery;

SWIR = reflectance in the short wave infrared band.

To examine the accuracy of final water body maps generated with mNDWI, the MLC maps resulting in 1990, 2000, 2010, and 2020 were compared with the results of mNDWI in these years where overall accuracy were calculated.

2.7. Post-classification

The post-classification comparison change detection technique was then employed for comparing four classified images of land use and land cover in 1990, 2000, 2010, and 2020. This method visually explores the trend of change and is among the most suitable and commonly applied techniques to reveal the increase and decrease of changes in the study area using multispectral image data (Petropoulos, et al., 2015; Chouari, 2021). The percentages of gain or loss of classes are then determined for each change detection map with respect to the total area.

3. Results

The algorithm developed for selecting and evaluating the quality and separability of AOIs with the analysis of the spectral profiles of the classes, JM distance, and scattering ellipses parameters provided reliable accuracy of the training samples on the 2020 image. Its application ensured high separability and representativeness of samples in the construction of AOIs for the classes "Sparse vegetation" and "Bare land" in arid regions (Fig.2). The best average separation of JM distance was greater than 1414 and demonstrate a reliable separability accuracy of classes (Fig.2a). Two-dimensional feature space of scattering ellipses plot indicates that there is no significant overlap between AOIs, which means acceptable extent of samples separability (Fig. 2c)

Accuracy assessment was performed to evaluate the results of the MLC on 2020 Landsat images based on ground control points. The overall classification accuracy was 93%, with a Kappa index of 0.90. Overall accuracy of more than 70% and a Kappa coefficient of more than 0.85 are considered a successful classification (Talukdar, et al., 2020).

To separate the territories that have diversity in reflection corresponding to the defined land cover types in the study area, unsupervised classification using the cluster method was applied for 2020 satellite images (Fig. 3b). Satisfactory results could not be achieved via this technique because of the proximity of spectral reflections along the territory and the inability of the software as well as algorithms to complete the separation conditions. As a result, it is important to rely on vegetation indices to confirm the classification accuracy. The results of unsupervised SAVI-based classification are shown in Fig. 3c. The observed accuracy of the used unsupervised classification technique was up to 0.91 (considering the data of field sampling), indicating a successful classification. Additionally, we calculated the Kappa statistics; the calculated value was 0.89.

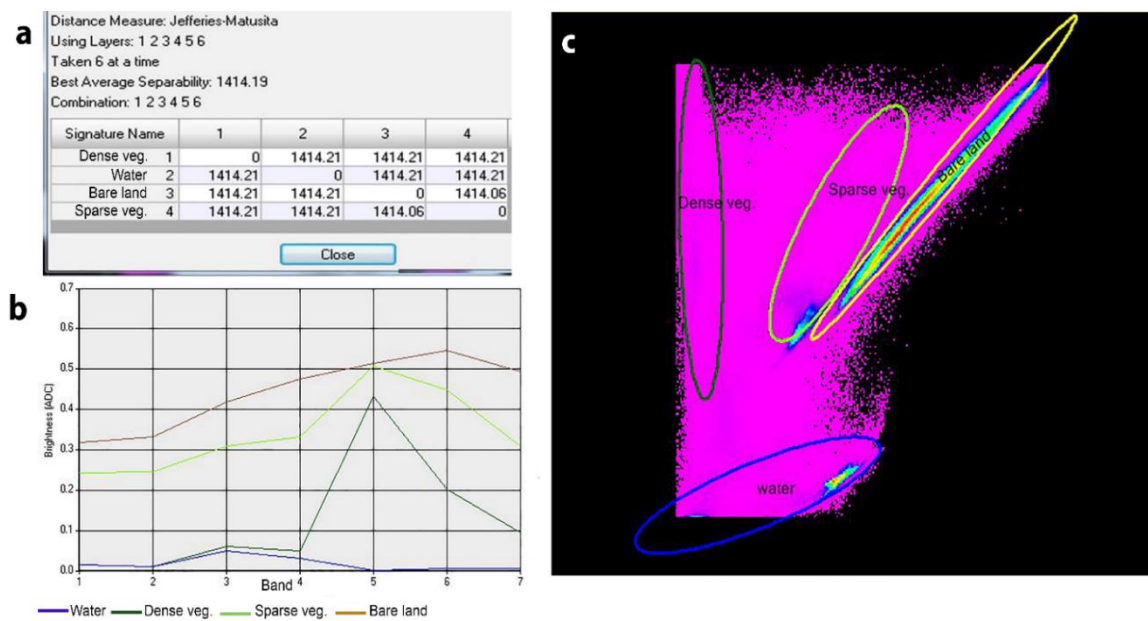


Fig. 2. a) Separability of AOIs based on JM distance; b) Spectral profiles of main land cover classes and c) assessing pixel deviation based on construction of scattering ellipses between NIR and Red channels in 2020 image

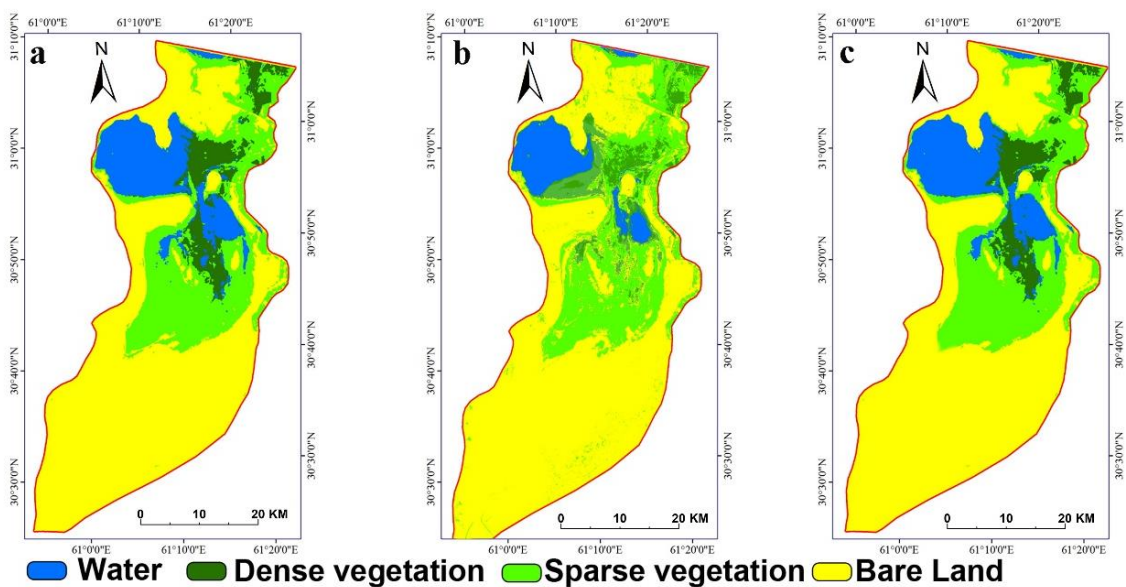


Fig. 3. The result of supervised classification (a), unsupervised classification (b), and unsupervised SAVI-based classification (c) in 2020.

Comparison of SAVI-based classification and MLC revealed that SAVI-based classification differentiated sparse vegetation and bare lands with acceptable accuracy. According to the results of SAVI mapping, unsupervised classification was performed for all scenes. The results of this SAVI-based classification are presented in Fig. 4b.

Table 3. The percentage of land cover types calculated for scenes of years 1990, 2000, 2010 and 2020 using unsupervised SAVI-based classification results.

Land Cover Type	1990	2000	2010	2020
Water	74.48 %	0	6.01%	10.85%
Bare land	23.6 %	88.3 %	87.68%	60.65%
Dense Vegetation	1.91 %	3.26 %	2.37%	6.22%
Sparse vegetation	0	8.44%	3.94%	22.86%

Additionally, the percentages of four selected land cover classes were calculated to estimate the LCCs that took place between the different times of image acquisition and to estimate the classification quality. For the unsupervised SAVI-based classification, we also mapped three classes of land cover in 1990 and 2000 plus four classes in 2010 and 2020 in our region (Fig. 4b). The results show that in the 1990 time series, water was the major land cover class, whereas in the 2000 time series, bare land was the main land cover. The final step was the accurate estimation of the SAVI-based unsupervised classification. As a benchmark for this quality estimation, the area percentage for each class was calculated using supervised classification results (Table 4). Comparison of Tables 3 and 4 shows that our methodology has been accurate enough to detect LCCs in dryland wetland ecosystems.

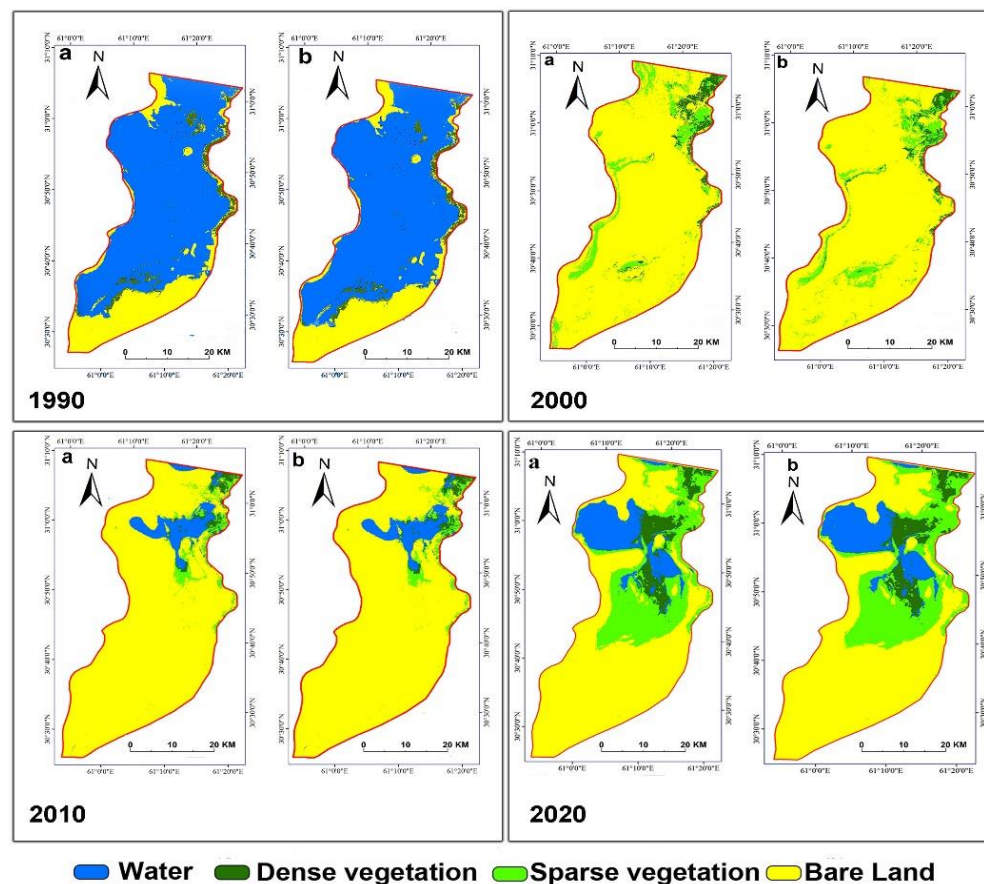


Fig. 4. The results of supervised classification(a), and unsupervised SAVI based classification (b) for all study times.

Table 4. The percentage of land cover types calculated for scenes of years 1990, 2000, 2010 and 2020 using supervised classification results

Land Cover Type	1990	2000	2010	2020
Water	74.81 %	0	5.8%	11.92%
Bare land	22.48 %	87.52 %	88.1%	59.08%
Dense Vegetation	2.71 %	3.88 %	2.3%	6.84%
Sparse vegetation	0	8.6%	3.8%	22.14%

As reported in Table 4, in 1990, water was the dominant land use type, covering 74.81% of the study area. However, the area of bare land increased in 2000, covering 87.52% of the study area, but decreased to 59.08% in 2020. Sparse vegetation increased from 0% in 1990 to 22% in 2020. This change shows that although the water class was subjected to a loss of about 69% in 2020, the vegetation cover class had grown by more than 20% in the wetland’s bottom. It is important to note that the vegetation cover is limited to humid areas (Fig. 4), where seasonal floods provide the necessary moisture.

Additionally, to understand the quantitatively temporal change of each classes and remaining ground cover unchanged in two periods of time, we use post classification comparison method. For this purpose, the mask of each class was placed on the classification results of the next period. Fig. 5 depicts the magnitude of LCCs in four time series over the entire study area.

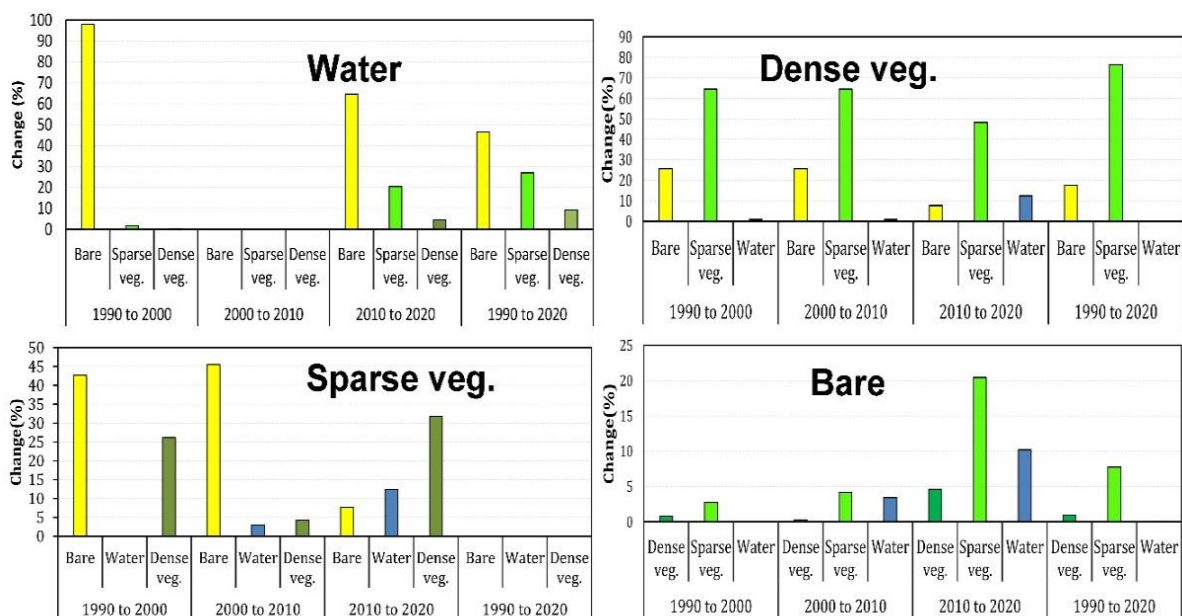


Fig. 5. Change (percentage of total area) in areas of land cover in the study area

The results indicate the dynamics of LCCs observed during a period of three decades. According to the results, between 1990 and 2000, severe drought caused the complete disappearance of water resources and transformed the water area into bare land (Fig. 5).

Annual fluctuations of water body in this wetland are shown in Fig. 6a. The error between non water in 1990, 2000, 2010, and 2020 MLC results and water body zone in mNDWI has

been 2.5%, 0%, 7.35%, and 6.69% respectively, which is acceptable to present a clear picture of yearly water body changes across the studied time series. Based on the results, before 2000, approximately 60 % of study area was dominated by water class and it was the major land cover in this wetland. After a severe drought in 2000, in most cases in subsequent years, the water body completely dried up. Comparison of the results of the annual changes in the area of water class with the amount of water inflow of Hirmand River to this lake (fig. 6b) shows that this lake is completely dependent on water sources in the outside of the basin. Between the 2000 and 2005, the studied area was totally dried, and the bare land was the major land cover of study area. From 2005 to 2008, because of spring floods, the area of the water class reached 10% of the entire border of the lake but dried in the period from 2008 to 2013, and this ecosystem experienced a severe dry-up where water area was zero. In the last 5 years of the study time, flood water has provided the required moisture for vegetation and this class grew up.

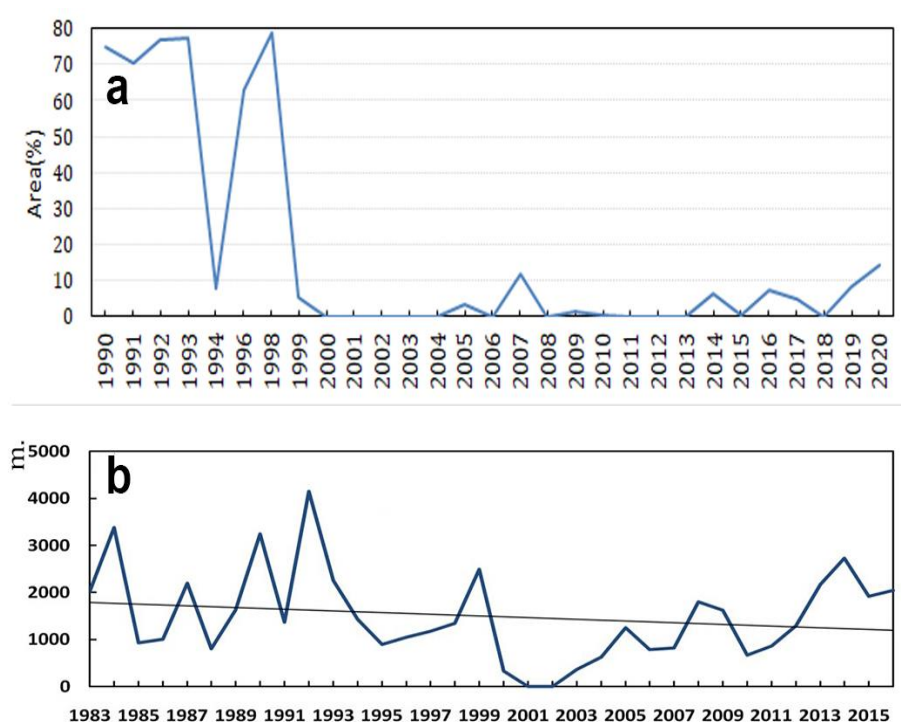


Fig. 6. Annual fluctuations of water body in Hamoun biosphere reserve using mNDWI (a) and Annual inflow of water (MCUM) through the river Hilmand (b)

4. Discussion

In this work, we used Landsat imagery to quantify LCCs in the Hamoun Biosphere Reserve, using pixel-based classification methods. Due to limited ground data for the study area, we performed MLC based on GCP's in 2020. The developed algorithm for selecting and evaluating the quality plus separability of AOIs with analyzing spectral profiles of classes ensured high efficiency of its application in creating training samples for automated classification of the study area. The training samples used in our methodology were taken using GCPs and spectral profiles. Accordingly, the pure pixels were detected for each class, based on which the neighbor pixels with similar spectral characteristics were selected for creating AOIs using "Region grow" properties tool in ERDAS Imagine. The accuracy of AOIs separability for each class was examined by JM distance criterion and scattering ellipse parameters. Our results revealed that

JM and scattering ellipses are useful for evaluating the separability of test and training class samples in the case of supervised pixel-based data classification. To detect LCCs over the past 30 years, a SAVI-based unsupervised classification method was used for classifying the same image in 2020. Comparison of the MLC and SAVI-based classification results showed an overall accuracy of 89% for our method. Comparing the results with other studies (Ajaj *et al.*, 2017; Mansourmoghaddam *et al.*, 2022) showed that this method provides the most optimal algorithm to monitoring LCC in the region without GCPs. Based on this method, other images from 1990, 2000, and 2010 were classified, and the spatial distribution of land use categories was extracted. The annual fluctuations of water area were calculated using mNDWI in GEE platform, and in this way, the changes across the time series of the studied area were investigated.

From 1990 to 2020, water volume diminished, causing a corresponding increase in the extent of grasslands (> 20%) and bare land (> 60%). From 1990 to 2000, surface water dominated the study area, accounting for a larger area than any other land cover in most of this decade. Over the second decade (2000–2010), despite the spring floods in some years and temporary accumulation of water in the northern part of the lake, the Hamoun Biosphere Reserve became almost completely dry, and bare land was the main land cover class. After that, surface water was restricted to the seasonal river delta, and along the last decade (2010–2020), grasslands were extensive and covered about 22% of the wetland's bottom.

Use of Landsat time-series indicated that after the 2000s, the southern part of the Lake became bare, and vegetation cover was limited to the northern areas, where seasonal floods bring sufficient moisture to ensure the survival of the vegetation. The results for the masked classes on the next time series showed that more than 90% of the water bodies was changed to bare land in the 2000s.

Comparing the changes of each class by masking them in 1990 and placing them on the classification results for the 2020s revealed that at the time of the study, more than 50% of the water-covered area changed to bare land, and approximately 30% of this class was replaced by a sparse vegetation cover. Our findings demonstrated that extremely high fluctuations occurred across the entire surface water areas.

The annual changes of the water class compared to the discharge of Hirmand River indicated that the survival of this biosphere reserve directly depends on water supply by this river.

More than 40% of the livelihood in this region directly depends on the pastures and the water bodies of the Hamoun Biosphere Reserve (Dahmardeh, *et al.*, 2009). The loss of moisture and the subsequent reduction in vegetation density directly affect the local economy (Sharifikia, *et al.*, 2013). Immigration and fuel smuggling is a clear example of the negative effects of lake drying-up on the local economy (Dahmardeh, *et al.*, 2012; Janparvar, *et al.*, 2017). Additionally, due to the strong winds in summer (Rashki, *et al.*, 2013; Hamidianpour, *et al.*, 2021), the dry bed of the lake becomes susceptible to dust storms, causing severe problems (Miri, *et al.*, 2007). In this context, LCC monitoring showed that the fragility of the Hamoun Biosphere Reserve environment has driven the ecological system to its current state, with far-reaching impacts on human life. Other studies shows that there is a linear relationship between the drying up of water bodies and increasing land surface temperature (Mansourmoghaddam *et al.*, 2023). this is the major point in the areas like Hamoun biosepher reserve that directly impacts on biodiversity

The purpose of this study was to monitor the LCCs of Hamoun Biosphere Reserve by detecting wetland cover changes. Although the remote sensing data and techniques proved valuable for LCC monitoring, to comprehensively examine the causes of LCC's, it is necessary to investigate the climatic parameters and river water discharge as well as to determine the contribution of each of these parameters.

5. Conclusions

The results of the satellite imagery classification were compared to identify the LCCs in the Hamoun Biosphere Reserve. Accuracy estimation of the classification results can be used as a measure of change detection reliability. Thus, the accuracy of image classification is highly important. Use of auxiliary data such as vegetation indices can improve the accuracy of unsupervised classification. According to our results, unsupervised classification cannot identify classes correctly because of the closeness of the reflectance. Numerical calculations of land cover based on supervised and unsupervised SAVI-based classification indicated that despite small differences among the obtained results, unsupervised SAVI-based classification could provide acceptable accuracy in this region.

Investigation of the minimum water requirement of the Hamoun Biosphere Reserve requires the study of all human, natural, and climatic factors of the Sistan Basin. It is necessary to revise the international laws in allocating the water right of this lake from the Hirmand River. Based on our results, there is a severe tendency for desertification in the study area. However, since the determination of the landscape changes requires a study with high accuracy, it is necessary to select an accurate method to determine phenomena using field data and appropriate vegetation indices for evaluating ecosystems.

References

- Abdollahi, A., Liu, Y., Pradhan, B., Huete, A., Dikshit, A., Tran, N.N., 2022. Short-time-series grassland mapping using Sentinel-2 imagery and deep learning-based architecture. *Egypt J Remote Sens Space Sci*, 25(3), 673-685. <https://doi.org/10.1016/j.ejrs.2022.06.002>
- Ahmad, A., Quegan, S., 2012. Analysis of maximum likelihood classification on multispectral data. *Applied Mathematical Sciences*. 6(129), 6425-36.
- Ahmed, K.R., Akter, S., Marandi, A., Schüth, C.A., 2021. Simple and robust wetland classification approach by using optical indices, unsupervised and supervised machine learning algorithms. *Remote Sens Appl Soc Environ*, 23, 100569. <https://doi.org/10.1016/j.rsase.2021.100569>
- Ajaj, Q.M., Pradhan, B., Noori, A.M., Jebur, M.N. 2017. Spatial monitoring of desertification extent in western Iraq using Landsat images and GIS. *Land Degradation & Development*, 28(8), 2418-2431.
- Alavi Zadeh, S., Monazzam Esmaeel Pour, A., Hossein Zadeh Kermani, M., 2013, Possibility study of areas with potential cultivation of saffron in Kashmar plain using GIS, *Saffron Agronomy & Technology*, 1 (1): 71-95. <https://doi.org/10.22048/jsat.2013.4812>
- Alavipanah, S.K., Amiri, R., Khodaei, K., 2007. The use of spectral signatures in extracting information from water quality parameters in the lake Urmia, Iran. *International Symposium on Physical Measurements and Signatures in Remote Sensing*, Davos, Switzerland. Available at: <https://www.isprs.org/proceedings/xxxvi/7-c50/papers/P76.pdf>
- Ali, M.Z., Qazi, W., Aslam, N., 2018. A comparative study of ALOS-2 PALSAR and landsat-8 imagery for land cover classification using maximum likelihood classifier. *The Egyptian Journal of Remote Sensing and Space Science*, 21, 29-35. <https://doi.org/10.1016/j.ejrs.2018.03.003>
- Alloghani, M., Al-Jumeily, D., Mustafina, J., Hussain, A., Aljaaf, A.J., 2020. A systematic review on supervised and unsupervised machine learning algorithms for data science. *Supervised and unsupervised learning for data science*. Springer, Cham, Switzerland, pp 3-21. https://doi.org/10.1007/978-3-030-22475-2_1
- Almalki, R., Khaki, M., Saco, P.M., Rodriguez, J.F., 2022. Monitoring and mapping vegetation cover changes in arid and semi-arid areas using remote sensing technology: a review. *Remote Sensing*, 14(20), 5143. <https://doi.org/10.3390/rs14205143>

- Alshahrani, H.M., Al-Wesabi, F.N., Al Duhayyim, M., Nemri, N., Kadry, S., Alqaralleh, B.A., 2021. An automated deep learning based satellite imagery analysis for ecology management. *Ecol Inform*, 66, 101452. <https://doi.org/10.1016/j.ecoinf.2021.101452>
- Bai, J., Chen, X., Li, J., Yang, L., Fang, H., 2011. Changes in the area of inland lakes in arid regions of central Asia during the past 30 years. *Environ Monit Assess*, 178(1), 247-256. <https://doi.org/10.1007/s10661-010-1686-y>
- Bashiri, M., Maroosi, M., Salari, A., Ghodoosi, M., 2018, Climatic zonation and land suitability determination for saffron in the Khorasan-Razavi province using data mining algorithms, *Saffron Agronomy & Technology*, 5 (4): 379-392. <https://doi.org/10.22048/jsat.2017.60768.1189>
- Berry, M.W., Mohamed, A., Yap, B.W., 2020. Supervised and unsupervised learning for data science, 1st ed, Springer Nature, pp 3-21. <https://doi.org/10.1007/978-3-030-22475-2>
- Bezerra, A.C., da Silva, J.L.B., de Albuquerque Moura, G.B., Lopes, P.M.O., Nascimento. C.R., et al., 2022. Dynamics of land cover and land use in Pernambuco (Brazil): Spatio-temporal variability and temporal trends of biophysical parameters. *Remote Sensing Applications: Society and Environment*, 25, 100677.
- Chen, H., Liu, H., Chen, X., Qiao, Y., 2020. Analysis on impacts of hydro-climatic changes and human activities on available water changes in Central Asia. *Science of the Total Environment*, 737, 139779.
- Chen, Y., Guerschman, J.P., Cheng, Z., Guo, L., 2019. Remote sensing for vegetation monitoring in carbon capture storage regions: A review. *Applied energy*, 240, 312-326.
- Chouari, W., 2021. Wetland land cover change detection using multitemporal Landsat data: a case study of the Al-Asfar wetland, Kingdom of Saudi Arabia. *Arab J Geosci*, 14(6), 1-14. <https://doi.org/10.1007/s12517-021-06815-y>
- Chughtai, A.H., Abbasi, H., Karas, I.R. 2021. A review on change detection method and accuracy assessment for land use land cover. *Remote Sensing Applications: Society and Environment*, 22, 100482.
- Condeça, J., Nascimento, J., Barreiras, N. 2022. Monitoring the storage volume of water reservoirs using Google Earth Engine. *Water Resources Research*, 58(3), e2021WR030026. <https://doi.org/10.1029/2021WR030026>
- Dabboor, M., Howell, S., Shokr, M., Yackel, J., 2014. The Jeffries–Matusita distance for the case of complex Wishart distribution as a separability criterion for fully polarimetric SAR data. *International Journal of Remote Sensing*, 35(19), 6859-6873. DOI: [10.1080/01431161.2014.960614](https://doi.org/10.1080/01431161.2014.960614)
- Dahmardeh, M., Piri, I., 2012. Importance of Hamoon Lake on rural development in Sistan region. *Am J Econ*, 2(6), 96-100. DOI: [10.5923/j.economics.20120206.01](https://doi.org/10.5923/j.economics.20120206.01)
- Dahmardeh, M., Shahraki, J., Akbari, A., 2019. Economic assessment of environmental damages caused by drying up of Hamoon wetland in Sistan region. *Journal of Natural Environmental Hazards*, 8(19), 209-228. DOI: [10.22111/jneh.2018.22176.1321](https://doi.org/10.22111/jneh.2018.22176.1321)
- Dahmardeh, M., Yazdani, S., Piri, E., 2009. The socio-economic effects of Hamoon lake in Sistan region of Iran. *J Food Agric Environ*, 7(2), 799-802.
- Dhingra, S., Kumar, D., 2019. A review of remotely sensed satellite image classification. *International Journal of Electrical and Computer Engineering*, 9(3), 1720. doi: [10.11591/ijece.v9i3.pp.1720-1731](https://doi.org/10.11591/ijece.v9i3.pp.1720-1731)
- Ehsani, A.H., Shakeryari, M., 2021. Monitoring of wetland changes affected by drought using four Landsat satellite data and Fuzzy ARTMAP classification method (case study Hamoun wetland, Iran). *Arabian Journal of Geosciences*, 14, 1-14. <https://doi.org/10.1007/s12517-020-06320-8>

- Gaikwad, S.V., Vibhute, A.D., Kale, K.V., Dhumal, R.K., Nagne, A.D., Mehrotra, S.C., Varpe, A.B., Surase, R.R., 2019. Drought severity identification and classification of the land pattern using Landsat 8 data based on spectral indices and maximum likelihood algorithm. *Microelectronics, Electromagnetics and Telecommunications*, Springer, Singapore, pp 517-524. https://doi.org/10.1007/978-981-13-1906-8_53
- Gao, L., Wang, X., Johnson, B.A., Tian, Q., Wang, Y., et al., 2020. Remote sensing algorithms for estimation of fractional vegetation cover using pure vegetation index values: A review. *ISPRS J Photogramm Remote Sens*, 159, 364-377. <https://doi.org/10.1016/j.isprsjprs.2019.11.018>
- Gill, T., Collett, L., Armston, J., Eustace, A., Danaher, T., Scarth, P., Flood, N., Phinn, S., 2010. Geometric correction and accuracy assessment of Landsat-7 ETM+ and Landsat-5 TM imagery used for vegetation cover monitoring in Queensland, Australia from 1988 to 2007. *J Spat Sci*, 55(2), 273-87. <https://doi.org/10.1080/14498596.2010.521977>
- Gong, P., Wang, J., Yu, L., Zhao, Y., Zhao, Y., et al., 2013. Finer resolution observation and monitoring of global land cover: First mapping results with Landsat TM and ETM+ data. *Int. J Remote Sens*, 34(7), 2607-2654. <https://doi.org/10.1080/01431161.2012.748992>
- Groisman, P., Bulygina, O., Henebry, G., Speranskaya, N., Shiklomanov, A., et al., 2018. Dryland belt of Northern Eurasia: contemporary environmental changes and their consequences. *Environ Res Lett*, 13(11), 115008. <https://doi.org/10.1088/1748-9326/aae43c>
- Hamidianpour, M., Jahanshahi, S.M.A., Kaskaoutis, D.G., Rashki, A., Nastos, P.G., 2021. Climatology of the Sistan Levar wind: At-mospheric dynamics driving its onset, duration and withdrawal. *Atmos Res*, 260, 105711. <https://doi.org/10.1016/j.atmosres.2021.105711>
- Hansen, M.C., Loveland, T.R., 2012. A review of large area monitoring of land cover change using Landsat data. *Remote sensing of Environment*, 122, 66-74.
- Huete, A.R. 1988. A soil-adjusted vegetation index (SAVI). *Remote sensing of environment*, 25(3), 295-309.
- Janparvar, M., Salehabadi, R., Zargari, M., 2017. Migration crisis caused by short-term droughts in Sistan and Baluchistan province. *Geography*, 15(52), 183-199.
- Jensen, J.R., 2018. *Introductory digital image processing: a Remote sensing perspective* (Pearson series in geographic information science) 4th Edition, Prentice-Hall Inc, UK.
- Jiang, H., Xu, X., Guan, M., Wang, L., Huang, Y., Jiang, Y., 2015. Determining the contributions of climate change and human activities to vegetation dynamics in agro-pastoral transitional zone of northern China from 2000 to 2015. *Sci Total Environ*, 718, 134871. <https://doi.org/10.1016/j.scitotenv.2019.134871>
- Jiang, Z., Jiang, W., Ling, Z., Wang, X., Peng, K., Wang, C., 2021. Surface water extraction and dynamic analysis of baiyangdian lake based on the google earth engine platform using sentinel-1 for reporting sdg 6.6. 1 indicators. *Water*, 13(2), 138. <https://doi.org/10.3390/w13020138>
- Kalidhas, M., Sivakumar, R., 2022. Image processing and Supervised Classification of LANDSAT data for Flood Impact Assessment on Land Use and Land Cover. 2nd International Conference on Technological Advancements in Computational Sciences (ICTACS), 437-440, IEEE. doi: 10.1109/ICTACS56270.2022.9988164.
- Kang, S., Lee, G., Togtokh, C., Jang, K., 2015. Characterizing regional precipitation-driven lake area change in Mongolia. *Journal of Arid Land*, 7, 146-158. <https://doi.org/10.1007/s40333-014-0081-x>
- Karkon Varnosfaderani, M., Kharazmi, R., Nazari Samani, A., Rahdari, M.R., Matinkhah, S.H., Aslinezhad, N., 2017. Distribution changes of woody plants in Western Iran as monitored by remote sensing and geographical information system: a case study of Zagros forest. *J For Res*, 28(1), 145-153. <https://doi.org/10.1007/s11676-016-0295-1>

- Karmaoui, A., Messouli, M., Khebiza, Y.M., Ifaadassan, I., 2014. Environmental vulnerability to climate change and anthropogenic impacts in dryland,(pilot study: Middle Draa Valley, South Morocco). *J Earth Sci Clim Change*, 11, 002. <http://dx.doi.org/10.4172/2157-7617.S11-002>
- Kaselimi, M., Voulodimos, A., Daskalopoulos, I., Doulamis, N., Doulamis, A., 2022. A vision transformer model for convolution-free multilabel classification of satellite imagery in deforestation monitoring. *IEEE Transactions on Neural Networks and Learning Systems*. doi: 10.1109/TNNLS.2022.3144791.
- Kennedy, R.E., Townsend, P.A., Gross, J.E., Cohen, W.B., Bolstad, P., Wang, Y.Q., Adams, P., 2009. Remote sensing change detection tools for natural resource managers: Understanding concepts and tradeoffs in the design of landscape monitoring projects. *Remote Sens Environ*, 113(7), 1382-1396. <https://doi.org/10.1016/j.rse.2008.07.018>
- Khalid, H.W., Khalil, R.M.Z., Qureshi, M.A. 2021. Evaluating spectral indices for water bodies extraction in western Tibetan Plateau. *The Egyptian Journal of Remote Sensing and Space Science*, 24(3), 619-634. <https://doi.org/10.1016/j.ejrs.2021.09.003>
- Kharazmi, R., Panidi, E.A., Karkon, V.M. 2016. Assessment of dry land ecosystem dynamics based on time series of satellite images. *Sovremennye problemy distantsionnogo zondirovaniya Zemli iz kosmosa*, 13(5), 214-23. DOI: 10.21046/2070-7401-2016-13-5-214-223
- Kharazmi, R., Tavili, A., Rahdari, M.R., Chaban, L., Panidi, E., Rodrigo-Comino, J., 2018. Monitoring and assessment of seasonal land cover changes using remote sensing: a 30-year (1987–2016) case study of Hamoun Wetland, Iran. *Environ Monit Assess*, 190, 356 <https://doi.org/10.1007/s10661-018-6726-z>
- Kumar, S., Arya, S., 2021. Change detection techniques for land cover change analysis using spatial datasets: A review. *Remote Sensing in Earth Systems Sciences*, 4(3), 172-185. <https://doi.org/10.1007/s41976-021-00056-z>
- Li, W., Hsu, C.Y., 2020. Automated terrain feature identification from remote sensing imagery: a deep learning approach. *Int J Geogr Inf Sci*, 34(4), 637-660. <https://doi.org/10.1080/13658816.2018.1542697>
- Li, J., Pei, Y., Zhao, S., Xiao, R., Sang, X., Zhan, C., 2020. A review of remote sensing for environmental monitoring in China. *Remote Sensing*, 12(7), 1130.
- Li, Q., Zhang, C., Shen, Y., Jia, W., Li, J., 2016. Quantitative assessment of the relative roles of climate change and human activities in desertification processes on the Qinghai-Tibet Plateau based on net primary productivity. *Catena*, 147, 789-796.
- Liu, H., Gong, P., Wang, J., Clinton, N., Bai, Y., Liang, S., 2020. Annual dynamics of global land cover and its long-term changes from 1982 to 2015. *Earth Syst Sci Data*, 12(2), 1217-1243. <https://doi.org/10.5194/essd-12-1217-2020>
- Liu, P., 2015. A survey of remote-sensing big data. *Front Environ Sci*, 3, 45. <https://doi.org/10.3389/fenvs.2015.00045>
- Long, W., Srihann, S., 2004. Land cover classification of SSC image: unsupervised and supervised classification using ERDAS Imagine, *Geosci. Remote. Sens. Lett. IEEE International Geoscience and Remote Sensing Symposium*, 4, 2707-2712. <https://doi.org/10.1109/IGARSS.2004.1369859>
- Lu, S., Wang, Y., Zhou, J., Hughes, A.C., Li, M., et al., 2022. Active water management brings possibility restoration to degraded lakes in dryland regions: a case study of Lop Nur, China. *Scientific Reports*, 12(1), 18578. <https://doi.org/10.1038/s41598-022-23462-9>
- Lv, Z., Huang, H., Li, X., Zhao, M., Benediktsson, J.A., Sun, W., Falco, N., 2022. Land cover change detection with heterogeneous remote sensing images: Review, progress, and perspective. *Proceedings of the IEEE*, 110(12), 1976-1991. doi: 10.1109/JPROC.2022.3219376.

- Maas, S.J., Nithya, R., 2010. Normalizing and Converting Image DC Data Using Scatter Plot Matching. *Remote Sensing* 2(7), 1644-1661. <https://doi.org/10.3390/rs2071644>
- Maleki, S., Koupaei, S.S., Soffianian, A., Saatchi, S., Pourmanafi, S., Rahdari, V., 2019. Human and climate effects on the Hamoun wetlands. *Weather Clim Soc*, 11(3), 609-622. <https://doi.org/10.1175/WCAS-D-18-0070.1>
- Malinowski, R., Lewiński, S., Rybicki, M., Gromny, E., Jenerowicz, M., Krupiński, M., Nowakowski, A., Wojtkowski, C., Krupiński, M., Krätzschar, E., Schauer, P., 2020. Automated production of a land cover/use map of Europe based on Sentinel-2 imagery. *Remote Sensing*, 12(21), 3523. <https://doi.org/10.3390/rs12213523>
- Mansourmoghaddam, M., Ghafarian Malamiri, H.R., Rousta, I., Olafsson, H., Zhang, H. 2022. Assessment of Palm Jumeirah Island's construction effects on the surrounding water quality and surface temperatures during 2001–2020. *Water*, 14(4), 634.
- Mansourmoghaddam, M., Rousta, I., Zamani, M., Mokhtari, M. H., Karimi Firozjahi, M., Alavipanah, S. K. 2021. Study and prediction of land surface temperature changes of Yazd city: assessing the proximity and changes of land cover, *Journal of RS and GIS for Natural Resources*, 12(4), 1-27. doi: 10.30495/girs.2021.682083
- Mansourmoghaddam, M., Rousta, I., Zamani, M., Olafsson, H. 2023. Investigating and predicting Land Surface Temperature (LST) based on remotely sensed data during 1987–2030 (A case study of Reykjavik city, Iceland). *Urban Ecosystems*, 1-23.
- Mason, I.M., Guzkowska, M.A.J., Rapley, C.G., 1994. The response of lake levels and areas to climatic change. *Clim Change*, 27, 161–197. <https://doi.org/10.1007/BF01093590>
- Miri, A., Ahmadi, H., Ghanbari, A., Moghaddamnia, A., 2007. Dust storms impacts on air pollution and public health under hot and dry climate. *Int J Energy Environ Eng*, 2(1), 101-105.
- Mishra, V.N., Prasad, R., Kumar, P., Gupta, D.K., Srivastava, P.K., 2017. Dual-polarimetric C-band SAR data for land use/land cover classification by incorporating textural information. *Environmental Earth Sciences*, 76(1), 1-16. <https://doi.org/10.1007/s12665-016-6341-7>
- Mohammady, M., Moradi, H.R., Zeinivand, H., Temme, A.J.A.M., 2015. A comparison of supervised, unsupervised and synthetic land use classification methods in the north of Iran. *Int J Environ Sci Technol*, 12(5), 1515-1526. <https://doi.org/10.1007/s13762-014-0728-3>
- Mousavi, S.A., Fakhireh, A., Shahryari, A., 2014. Assessment of changes trend of land cover with use of remote sensing data in Hamoon wetlands. *J Biodivers Conserv Environ Sci*, 4(5), 146-156.
- Mousazadeh, R., Ghaffarzadeh, H., Nouri, J., Gharagozlou, A., Farahpour, M., 2015. Land use change detection and impact assessment in Anzali international coastal wetland using multi-temporal satellite images. *Environ Monit Assess*, 187(12), 1-11. <https://doi.org/10.1007/s10661-015-4900-0>
- Muttitanon, W., Tripathi, N.K., 2005. Land use/land cover changes in the coastal zone of Ban Don Bay, Thailand using Landsat 5 TM data. *Int J Remote Sens*, 26(11), 2311-23. <https://doi.org/10.1080/0143116051233132666>
- Nagendra, H., Lucas, R., Honrado, J.P., Jongman, R.H., Tarantino, C., Adamo, M., Mairota, P., 2013. Remote sensing for conservation monitoring: Assessing protected areas, habitat extent, habitat condition, species diversity, and threats. *Ecol Indic*, 33, 45-59. <https://doi.org/10.1016/j.ecolind.2012.09.014>
- Nutini, F., Boschetti, M., Brivio, P.A., Bocchi, S., Antoninetti, M., 2013. Land-use and land-cover change detection in a semi-arid area of Niger using multi-temporal analysis of Landsat images. *International journal of remote sensing*, 34(13), 4769-4790. <https://doi.org/10.1080/01431161.2013.781702>

- Opedes, H., Múcher, S., Baartman, J.E., Nedala, S., Mugagga, F., 2022. Land Cover Change Detection and Subsistence Farming Dynamics in the Fringes of Mount Elgon National Park, Uganda from 1978–2020. *Remote Sensing*, 14(10), 2423. <https://doi.org/10.3390/rs14102423>
- Othman, Y., Steele, C., St Hilaire, R., 2018. Surface Reflectance Climate Data Records (CDRs) is a reliable Landsat ETM+ source to study chlorophyll content in pecan orchards. *J Indian Soc Remote Sens*, 46(2), 211-218. <https://doi.org/10.1007/s12524-017-0690-x>
- Pande, C.B., 2022. Land use/land cover and change detection mapping in Rahuri watershed area (MS), India using the google earth engine and machine learning approach. *Geocarto International*, 1-21. <https://doi.org/10.1080/10106049.2022.2086622>
- Pandey, P.C., Koutsias, N., Petropoulos, G.P., Srivastava, P.K., Ben Dor, E., 2021. Land use/land cover in view of earth observation: data sources, input dimensions, and classifiers—a review of the state of the art. *Geocarto International*, 36(9), 957-988. <https://doi.org/10.1080/10106049.2019.1629647>
- Petropoulos, G.P., Kalivas, D.P., Griffiths, H.M., Dimou, P.P., 2015. Remote sensing and GIS analysis for mapping spatio-temporal changes of erosion and deposition of two Mediterranean river deltas: The case of the Axios and Aliakmonas rivers, Greece. *Int J of Applied Earth Observation and Geoinformation*, 35, 217-228. <https://doi.org/10.1016/j.jag.2014.08.004>
- Rad, A.M., Kreitler, J., Sadegh, M., 2021. Augmented Normalized Difference Water Index for improved surface water monitoring. *Environ Model Softw*, 140, 105030. <https://doi.org/10.1016/j.envsoft.2021.105030>
- Rahimi, A., Breuste, J., 2021. Why is Lake Urmia drying up? Prognostic modeling with land-use data and artificial neural network. *Frontiers in Environmental Science*, 9, 603916. <https://doi.org/10.3389/fenvs.2021.603916>
- Rashki, A., Kaskaoutis, D.G., Goudie, A.S., Kahn, R.A., 2013. Dryness of ephemeral lakes and consequences for dust activity: the case of the Hamoun drainage basin, southeastern Iran. *Sci Total Environ*, 463, 552-564. <https://doi.org/10.1016/j.scitotenv.2013.06.045>
- Rastegar-Pouyani, N., Gholamifard, A., Karamiani, R., Bahmani, Z., Mobaraki, A., Abtin, E., Faizi, H., Heidari, N., Takesh, M., Sayyadi, F., Ahsani, N., Browne, R.K. 2015. Sustainable Management of the Herpetofauna of the Iranian Plateau and coastal Iran. *Amphib Reptile Conserv*, 9(1), 1-15.
- Rezaei, R., & Ghofranfarid, M. 2018. Rural households' renewable energy usage intention in Iran: extending the unified theory of acceptance and use of technology. *Renewable Energy*, 122, 382–391.
- Rousta, I., Sarif, M.O., Gupta, R.D., Olafsson, H., Ranagalage, M., Murayama, Y., Zhang, H., Mushore, T.D. 2018. Spatiotemporal analysis of land use/land cover and its effects on surface urban heat island using Landsat data: A case study of Metropolitan City Tehran (1988–2018). *Sustainability*, 10(12), 4433.
- Sahabi, H., Moallem Banhangi, F., 2022, Evaluation the Impact Climatic Parameters on Flowering Behaviour and Yield Of Saffron (*Crocus sativus* L.) in Razavi and Southern Khorasan Provinces, *Saffron Agronomy & Technology*, 9 (4), 357-373. <https://doi.org/10.22048/jsat.2021.283088.1423>
- Sanadgol, M., Asghari Lafmejani, S., Fazelnia, G., Pirani, M., 2022. Physical and environmental constraints of entrepreneurship in the villages surrounding the border and Hamoon International Wetland (The study of District Ghorghori, Hirmand County). *Journal of Studies in Entrepreneurship and Sustainable Agricultural Development*, 9(2), 37-58. doi: 10.22069/jead.2022.19746.1552
- Şerban, R.,D., Jin, H., Şerban, M., Luo, D., Wan, Q., Jin, X., Ma, Q., 2020. Mapping thermokarst lakes and ponds across permafrost landscapes in the headwater area of yellow river on northeastern Qinghai-Tibet plateau. *Int J Remote Sens*, 41, 7042–7067. <https://doi.org/10.1080/01431161.2020.1752954>

- Sharifikia, M., 2013. Environmental challenges and drought hazard assessment of Hamoun Desert Lake in Sistan region, Iran, based on the time series of satellite imagery. *Natural hazards*, 65(1), 201-217. <https://doi.org/10.1007/s11069-012-0353-8>
- Soliman, G.A.A., Soussa, H., 2011. Wetland change detection in Nile swamps of southern Sudan using multitemporal satellite imagery. *J Appl Remote Sens*, 5(1), 053517. <https://doi.org/10.1117/1.3571009>
- Sonnenschein, R., Kuemmerle, T., Udelhoven, T., Stellmes, M., Hostert, P., 2011. Differences in Landsat-based trend analyses in dry-lands due to the choice of vegetation estimate. *Remote Sens Environ*, 115(6), 1408-1420. <https://doi.org/10.1016/j.rse.2011.01.021>
- Stavi, I., Pulido Fernández, M., Argaman, E. 2023. Long-term passive restoration of severely degraded drylands—divergent impacts on soil and vegetation: An Israeli case study. *Journal of Geographical Sciences*, 33(3), 529-546.
- Swain, P.H., Davis, S.M. 1978. *Remote Sensing: The Quantitative Approach*. New York: McGraw-Hill.
- Tahsin, S., Medeiros, S.C., Singh, A., 2021. Consistent Long-Term Monthly Coastal Wetland Vegetation Monitoring Using a Virtual Satellite Constellation. *Remote Sens*, 13(3), 438. <https://doi.org/10.3390/rs13030438>
- Talukdar, S., Mankotia, S., Shamimuzzaman, M., Mahato, S., 2021. Wetland-inundated area modeling and monitoring using supervised and machine learning classifiers. *Advances in Remote Sensing for Natural Resource Monitoring*, 5, 346-365. <https://doi.org/10.1002/9781119616016.ch17>
- Talukdar, S., Singha, P., Mahato, S., Pal, S., Liou, Y.A., Rahman, A., 2020. Land-use land-cover classification by machine learning classifiers for satellite observations—A review. *Remote Sensing*, 12(7), 1135. <https://doi.org/10.3390/rs12071135>
- Tmušić, G., Manfreda, S., Aasen, H., James, M.R., Gonçalves, G., et al., 2020. Current practices in UAS-based environmental monitoring. *Remote Sensing*, 12(6), 1001. <https://doi.org/10.3390/rs12061001>
- Vekerdy, Z., Dost, R.J.J., Reinink, G., Partow, H., 2006. History of environmental change in the Sistan Basin based on satellite image analysis: 1976-2005. *UNEP Post-Conflict Branch Geneva*, <https://wedocs.unep.org/20.500.11822/7690>
- Venter, Z.S., Scott, S.L., Desmet, P.G., Hoffman, M.T., 2020. Application of Landsat-derived vegetation trends over South Africa: Potential for monitoring land degradation and restoration. *Ecol Indic*, 113,106206. <https://doi.org/10.1016/j.ecolind.2020.106206>
- Viennois, G., Proisy, C., Feret, J.B., Prospero, J., Sidik, F., Rahmania, R., Longépé, N., Germain, O., Gaspar, P., 2016. Multitemporal analysis of high-spatial-resolution optical satellite imagery for mangrove species mapping in Bali, Indonesia. *IEEE Journal of Selected Topics in Applied Earth Observations and Remote Sensing*, 9(8), 3680-3686. [10.1109/JSTARS.2016.2553170](https://doi.org/10.1109/JSTARS.2016.2553170)
- Wang, L., Diao, C., Xian, G., Yin, D., Lu, Y., Zou, S., Erickson, T.A., 2020. A summary of the special issue on remote sensing of land change science with Google earth engine. *Remote Sensing of Environment*, 248,112002. <https://doi.org/10.1016/j.rse.2020.112002>
- Wang, S., He, Y., Hu, S., Ji, F., Wang, B., Guan, X., Piccolroaz, S., 2021. Enhanced warming in global dryland lakes and its drivers. *Remote Sens*, 14(1), 86. <https://doi.org/10.3390/rs14010086>
- Wang, Y., Ma, J., Xiao, X., Wang, X., Dai, S., Zhao, B., 2019. Long-term dynamic of Poyang Lake surface water: A mapping work based on the Google Earth Engine cloud platform. *Remote Sensing*, 11(3), 313. <https://doi.org/10.3390/rs11030313>

- Wulder, M.A., Roy, D.P., Radeloff, V.C., Loveland, T.R., Anderson, M.C., et al., 2022. Fifty years of Landsat science and impacts. *Remote Sensing of Environment*, 280, 113195. doi: 10.1016/j.rse.2022.113195
- Xie, S., Liu, L., Zhang, X., Yang, J., 2022. Mapping the annual dynamics of land cover in Beijing from 2001 to 2020 using Landsat dense time series stack. *ISPRS Journal of Photogrammetry and Remote Sensing*, 185, 201-218.
- Xu, D., Song, A., Li, D., Ding, X., Wang, Z., 2019. Assessing the relative role of climate change and human activities in desertification of North China from 1981 to 2010. *Frontiers of Earth Science*, 13, 43-54. <https://doi.org/10.1007/s11707-018-0706-z>
- Xu, H., 2006. Modification of normalised difference water index (NDWI) to enhance open water features in remotely sensed imagery. *International journal of remote sensing*, 27(14), 3025-3033.
- Xu, Z., Xu, S., Qian, C., Klette, R., 2019. Accurate ellipse extraction in low-quality images. 16th International Conference on Machine Vision Applications (MVA), IEEE, pp. 1-5. doi: 10.23919/MVA.2019.8757970
- Yang, L., Driscoll, J., Sarigai, S., Wu, Q., Chen, H., Lippitt, C.D., 2022. Google earth engine and artificial intelligence (ai): a comprehensive review. *Remote Sensing*, 14(14), 3253. <https://doi.org/10.3390/rs14143253>
- Yang, X., Lo, C.P., 2022. Using a time series of satellite imagery to detect land use and land cover changes in the Atlanta, Georgia metropolitan area. *Int J Remote Sens*, 23 (9),1775–1798. doi:10.1080/01431160110075802
- Yang, X., Wang, N., He, J., Hua, T., Qie, Y., 2020. Changes in area and water volume of the Aral Sea in the arid Central Asia over the period of 1960–2018 and their causes. *Catena*, 191, 104566. <https://doi.org/10.1016/j.catena.2020.104566>
- Yousefi, S., Mirzaee, S., Almohamad, H., Al Dughairi, A.A., Gomez, C., Siamian, N., Alrasheedi, M., Abdo H.G., 2022. Image classification and land cover mapping using sentinel-2 imagery: optimization of SVM parameters. *Land*, 11(7), 993. <https://doi.org/10.3390/land11070993>
- Yuan, F., Sawaya, K.E., Loeffelholz, B.C., Bauer, M.E., 2005. Land cover classification and change analysis of the Twin Cities (Min-nesota) Metropolitan Area by multitemporal Landsat remote sensing. *Remote Sens Environ*, 98(2-3), 317-328. <https://doi.org/10.1016/j.rse.2005.08.006>
- Yuan, Q., Shen, H., Li, T., Li, Z., Li, S., Jiang, Y., Xu, H., Tan, W., Yang, Q., Wang, J., Gao, J., 2020. Deep learning in environmental remote sensing: Achievements and challenges. *Remote Sensing of Environment*, 241, 111716.
- Zhai, M., 2019. Inversion of organic matter content in wetland soil based on Landsat 8 remote sensing image. *J Vis Commun Image Represent*, 64,102645. <https://doi.org/10.1016/j.jvcir.2019.102645>
- Zhai, Y., Roy, D.P., Martins, V.S., Zhang, H.K., Yan, L., Li, Z., 2022. Conterminous United States Landsat-8 top of atmosphere and surface reflectance tasseled cap transformation coefficients. *Remote Sensing of Environment*, 274, 112992. doi: 10.1016/j.rse.2022.112992
- Zhao, Y., Su, D., Bao, Y., Yang, W., Zhao, C., Bai, Y., Zhao, Y., 2017. Dynamic monitoring of fractional vegetation cover of eco-function area of grassland on northern foot of Yinshan Mountains through remote sensing technology. *Res Environ Sci*, 30(2), 240-248. <http://dx.doi.org/10.13198/j.issn.1001-6929.2017.01.35>
- Zhu, Y., Zhang, Y., Zheng, Z., Liu, Y., Wang, Z., et al., 2022. Converted vegetation type regulates the vegetation greening effects on land surface albedo in arid regions of China. *Agricultural and Forest Meteorology*, 324, 109119.

Zhu, Z., Zhang, J., Yang, Z., Aljaddani, A.H., Cohen, W.B., Qiu, S., Zhou, C., 2020. Continuous monitoring of land disturbance based on Landsat time series. *Remote Sens Environ*, 238, 111-116. <https://doi.org/10.1016/j.rse.2019.03.009>